A reduced-order model of squeeze-film damping for deformable micromechanical structures including large displacement effects

Alexia Missoffe, Jérôme Juillard, Denis Aubry

To cite this version:

HAL Id: hal-00270341

https://centralesupelec.hal.science/hal-00270341v2

Submitted on 21 Jan 2009

A reduced-order model of squeeze-film damping for deformable micromechanical structures including large displacement effects

Abstract: we present a reduced-order model of the squeezed-film damping phenomenon which is valid for flexible structures, large displacements (with respect to the gap) and small pressure variations (with respect to the ambient pressure). This reduced-order model is obtained by transforming the Reynolds equation into a form more amenable to modal projection techniques. Our approach is validated by comparison to simulated and experimental data. Moreover, we show that in several practical cases the "small pressure" hypothesis is not limitative, even when the gap becomes very small.

I Introduction

Correct modelling of damping is essential to capture the dynamic behaviour of a MEMS device. At ambient or moderately low pressure, the major dissipation phenomenon is usually fluid damping: squeeze-film damping when the micromechanical structure moves perpendicular to the substrate, slide-film damping when it moves parallel to the substrate and viscous drag when it is far from the substrate. In the present paper, we focus our attention on squeeze-film damping which models the behaviour of a fluid in small gaps between a fixed surface and a structure moving perpendicular to this surface. The lateral dimensions of the surfaces are large compared to the gap, the system is considered isothermal and the effects of inertia are small compared to those of viscosity. Squeeze film damping is then governed by the Reynolds equation:

$$\nabla(\frac{G^3}{12\mu}P\nabla P) = \frac{\partial GP}{\partial t}, \quad (1)$$

where $G(x, y, t)$ is the distance between the moving and the fixed surface, $P(x, y, t)$ is the pressure, and μ is the effective viscosity of the fluid [1]. For small excitation frequencies or amplitudes the squeezed film behaves as a linear damper. For larger amplitudes or frequencies, the gas has no time to flow away and the pressure builds up creating a stiffening effect coupled to a nonlinear damping. The boundary conditions for (1) are usually chosen as trivial: "zero pressure variation" or "zero pressure gradient", although some authors have considered less ideal, frequency-dependent and aspect-ratio dependent boundary conditions [2-3]. A complete review on this equation and its different regimes can be found in [4].

Coupling the Reynolds equation to the equation governing the mechanical behaviour of the micromechanical structure leads to a nonlinear system of partial differential equations (PDEs). This system has no analytical solution and must be simplified with some assumptions. The most commonly made assumptions are the following:

- uniform displacements, i.e. $\frac{\partial G}{\partial x} = \frac{\partial G}{\partial y} = 0$ (for example, [5]).

- steady-state sinusoidal excitation, i.e. $G = G_e \sin(\omega t)$ [6-7].

- small displacements, i.e. $G = G_0 + g$ and $g << G_0$, where G_0 is the nominal gap of the structure at rest or close to a static equilibrium [8-9].

- small pressure variations, i.e. $P = P_0 + p$ and $p << P_0$, where P_0 is the ambient pressure.

These hypotheses prove to be useful in a variety of applications, if only for gaining insight of nonlinear damping phenomena. However, in many cases, it is difficult to justify their use: for example, it is clear to see that none of the first three hypotheses holds when trying to estimate the switching time of a micro-switch. Most micro-switches do not undergo uniform

displacements, nor can these displacements be considered small, and the behaviour of a micro-switch is fundamentally transient.

To date, the most notable attempts to tackle the problem of reduced-order modelling (ROM) of squeeze-film damping with large, non-uniform displacements have been made by Younis *et al.* [10-12], Mehner *et al.* [6,13], Yang *et al.* [14-15], Hung and Senturia [16] and Rewienski and White [17-18]. In [10-12], the authors propose to solve the nonlinear Euler-Bernoulli beam equation to determine the static deformation of a microplate under a voltage bias. The von Karman plate equations and the compressible Reynolds equation are then linearized close to this operating point and a perturbation method is used to calculate the pressure deviation. In [6,13], the authors use a modal projection method to calculate modal frequency-dependent damping and stiffening coefficients close to a determined operating point. To extend this approach to large displacements, Mehner [6] gives an analytical expression of these coefficients as a function of mechanical modal coordinates established by fitting of simulation data for different initial deformations. These approaches are all based on several steady-state sinusoidal calculations [10-12] or simulations [6,13], which increase the time for setting up the reduced-order model. The most general approaches may well be those developed in [14-18]: the authors rely on fully-coupled, nonlinear transient simulations of the complete system (usually a micro-switch) to establish a reduced-order model of the micromechanical structure. These approaches are very general and they can even be successfully applied to the fully nonlinear Reynolds equation (1). However, they have a high computational cost (because of the nonlinear/multiphysics/transient simulation they require) and their accuracy depends, to some degree, on the choice of the training trajectory.

In the present paper, we establish a semi-analytical reduced-order model of the Reynolds equation which is valid for large, non-uniform displacements and transient excitation of an arbitrarily-shaped micromechanical structure, but is limited to small pressure variations. This small pressure hypothesis is also made in the models developed by Younis *et al.*: however, the approaches developed in [10-12] are based on the assumption of large static deflections (under a bias voltage) and small dynamic deflections caused by a sinusoidal forcing. As a consequence, they are ideal for studying MEMS resonators but they cannot be used to investigate transient phenomena involving large dynamic deflections, such as the switching time of RF switches, for example, and, more generally, devices operating close to their pull-in point. The lack of a simple model for such common devices motivates the present work.

Note that assuming small pressure variations with respect to unity is not exactly the same as assuming incompressible flow (in which case, p/P_0 is assumed small compared to g/G_0 [4]). As a rule of thumb, one may restrain the validity of this approximation to moderately large squeeze numbers. Air rarefaction effects, such as slip-flow, may act in the opposite direction, as shown in [24], and increase the domain of validity of the small pressure hypothesis. The same goes for structures with holes, which, for a given excitation, undergo smaller pressure changes than structures without holes. For large-displacement, high-frequency excitation and/or very low ambient pressure, the present model should not be used.

The guiding idea of our work is to notice that the time-varying nature of the spatial differential operator of (1) makes modal projection methods unusable, because there exists no complete unchanging set of eigenfunctions on which to project the equation. In part II of the paper, we show how (1) can be transformed into a more tractable PDE through a change of variables: the main property of this resulting PDE is that its spatial differential operator does not depend on time and it is therefore amenable to modal projection techniques. We also show how the boundary conditions of the Reynolds equation are modified through the proposed change of variables and discuss the validity of the small pressure hypothesis. The results obtained with the reduced-order model and with a finite-difference model are compared. In part III, we show how this model of squeeze-film damping can be coupled to the model

governing the (electro-) mechanical behaviour of a micromechanical structure, such as a microswitch. We compare the resulting ROM to those obtained with other approaches, qualitatively as well as quantitatively, and discuss the effect of slip-flow and compressibility on the switching times of the device.

II A reduced-order model of squeeze-film damping based on modal projection

In this section, for the sake of simplicity, we assume that the effective viscosity of the fluid is constant and uniform: the case of a non-uniform effective viscosity, as in [14-18], is treated in section III-2.

1 Transformation of the Reynolds equation

Assuming small pressure variations with respect to the ambient pressure, the nonlinear Reynolds equation can be written:

$$\nabla\left(\frac{G^3}{12\mu}\nabla p\right) = \frac{\partial}{\partial t}\left(G\left(1+\frac{p}{P_0}\right)\right), \quad (2)$$

with $P = P_0 + p$. As we have pointed out in the introduction, the spatial differential operator appearing in (2) depends on time. Thus, unless G is separable in time and space, i.e. $G = \gamma(t)\Gamma(x,y)$, it appears difficult to find an unvarying basis of eigenmodes on which to project (2). We propose to transform (2) by introducing a "squeeze function" φ, through the following change of variables[1]:

$$p = \varphi G^{-3/2}. \quad (3)$$

The motivation for this change of variables is that it transforms (2) to a form where the spatial differential operator does not depend on time, and for which it is possible to find a fixed basis of eigenmodes. Using (3), and dividing by $G^{3/2}$, (2) can be rewritten as:

$$\Delta\varphi - \varphi\frac{\Delta G^{3/2}}{G^{3/2}} = \frac{12\mu}{G^{3/2}}\frac{\partial}{\partial t}\left(G\left(1+\frac{p}{P_0}\right)\right). \quad (4)$$

Using integration by parts, the right-hand side of (4) can be further transformed to:

$$\frac{12\mu}{G^{3/2}}\frac{\partial}{\partial t}\left(G\left(1+\frac{p}{P_0}\right)\right) = 12\mu\left[\frac{\partial}{\partial t}\left(G^{-1/2}\left(1+\frac{p}{P_0}\right)\right) - G\left(1+\frac{p}{P_0}\right)\frac{\partial G^{-3/2}}{\partial t}\right]. \quad (5)$$

Since we assume small pressure variations with respect to P_0, the second term on the right-hand side of (5) reduces to:

$$G\left(1+\frac{p}{P_0}\right)\frac{\partial G^{-3/2}}{\partial t} \approx G\frac{\partial G^{-3/2}}{\partial t} = -\frac{3}{2}G^{-3/2}\frac{\partial G}{\partial t} = 3\frac{\partial G^{-1/2}}{\partial t}, \quad (6)$$

and, thus, the transformed Reynolds equation becomes:

$$\Delta\varphi - \varphi\frac{\Delta G^{3/2}}{G^{3/2}} = 12\mu\frac{\partial}{\partial t}\left(-2G^{-1/2}+\frac{G^{-2}\varphi}{P_0}\right). \quad (7)$$

The spatial differential operator appearing in (7) is the Laplacian, the eigenmodes of which form a complete orthonormal basis that can be used to represent all the solutions of $\Delta\varphi = f$ [19]. Analytical expressions of these modes are available for a variety of geometries [20].
Now let us look at how trivial boundary conditions are transformed by (3). It is clear that:

$$p = 0 \Leftrightarrow \varphi = 0. \quad (8)$$

---

[1] A similar change of variables can also be found when accounting for slip-flow, as will be shown in section III.

Thus for an open boundary, the boundary condition remains unchanged. Let us now look at how the "no flux" boundary condition translates in terms of squeeze functions: letting $\vec{n}$ be the outward unit normal at the closed boundaries of the domain, we have:

$$\frac{\partial p}{\partial \vec{n}} = G^{-3/2} \frac{\partial \varphi}{\partial \vec{n}} + \varphi \frac{\partial G^{-3/2}}{\partial \vec{n}} = G^{-3/2} \frac{\partial \varphi}{\partial \vec{n}} - \frac{3}{2} \varphi G^{-5/2} \frac{\partial G}{\partial \vec{n}} = 0 . \qquad (9)$$

In most actual cases, the micromechanical structure is clamped at the closed boundaries. Therefore, the second term on the right-hand side of (9) vanishes and we have:

$$\frac{\partial p}{\partial \vec{n}} = 0 \Leftrightarrow \frac{\partial \varphi}{\partial \vec{n}} = 0 . \qquad (10)$$

In the following sub-section, we show how a reduced-order model can be constructed from (7), (8) and (10).

2 Construction of a reduced-order model

In order to apply a modal projection technique to (7), one looks for a solution of the following form:

$$\varphi^{(N)} = \sum_{k=1}^{N} s_k(t) \varphi_k(x,y) , \quad (11)$$

with

$$\Delta \varphi_k = -\lambda_k^{\,2} \varphi_k , \quad (12)$$

and where φ_k satisfies the same boundary conditions as φ. For example, in the case of a cantilever beam, defined by $(x,y) \in [0,L] \times [0,W]$, supposing the beam is clamped at $x=0$ and free at its other edges, the boundary conditions for φ_k are:

$$\begin{cases} \left. \dfrac{\partial \varphi_k}{\partial x} \right|_{x=0} = 0 \\ \varphi_k(x,0) = \varphi_k(x,W) = \varphi_k(L,y) = 0 \end{cases} , \qquad (13)$$

and, separating the variables in (12), one obtains:

$$\varphi_k(x,y) = \phi_{k_1,k_2}(x,y) = \frac{2}{\sqrt{LW}} \cos\!\left(\left(k_1 + \frac{1}{2} \right) \frac{\pi}{L} x \right) \sin\!\left(k_2 \frac{\pi}{W} y \right), \ k_1 \geq 0, k_2 \geq 1 . \qquad (14)$$

For complex geometries, the mode shapes may be found using FEM analysis, for example. Replacing φ in (7) by its expression (11) yields:

$$\sum_{k=1}^{N} s_k \varphi_k \left(-\lambda_k^2 - \frac{\Delta G^{3/2}}{G^{3/2}} \right) = 12\mu \frac{\partial}{\partial t} \left(-2G^{-1/2} + \frac{1}{P_0} \sum_{k=1}^{N} s_k \varphi_k G^{-2} \right), \qquad (15)$$

and projecting on the lth mode gives:

$$\sum_{k=1}^{N} s_k \left(-\lambda_k^2 \delta_{kl} - \left\langle \frac{\Delta G^{3/2}}{G^{3/2}} \varphi_k \middle| \varphi_l \right\rangle \right) = 12\mu \frac{d}{dt} \left(\left\langle -2G^{-1/2} \middle| \varphi_l \right\rangle + \frac{1}{P_0} \sum_{k=1}^{N} s_k \left\langle G^{-2} \varphi_k \middle| \varphi_l \right\rangle \right), \qquad (16)$$

where δ_{kl} stands for the Kronecker delta and the scalar product is defined by:

$$\langle f | g \rangle = \iint_{\Omega} fg \, dx dy , \qquad (17)$$

where Ω is the (two-dimensional) domain occupied by the air gap. This scalar product and the eigenmodes do not depend on time, which is why one may factor the time derivative on the right hand-side. One may rewrite (16) in matrix form:

$$\frac{d}{dt}(\mathbf{As}) = \frac{d}{dt}\mathbf{f} + \mathbf{Hs} , \qquad (18)$$

with

$$f_l = 24\mu \left\langle G^{-1/2} \middle| \varphi_l \right\rangle, \qquad (19)$$

$$H_{kl} = -\lambda_k^2 \delta_{kl} - \left\langle \frac{\Delta G^{3/2}}{G^{3/2}} \varphi_k \,\middle|\, \varphi_l \right\rangle, \qquad (20)$$

and

$$A_{kl} = \frac{12\mu}{P_0} \left\langle G^{-2} \varphi_k \,\middle|\, \varphi_l \right\rangle. \quad (21)$$

Because of the completeness argument mentioned in subsection II-1, the solution of the system of ordinary differential equations (18) defines squeeze coordinates in such a way that $\varphi^{(N)}$ converges to the solution of (7), as N goes to infinity. Small values of N will usually give a sufficiently good approximation of the solution of the original problem, as we will show in subsections II-3 and III-2.

Before proceeding to the coupling of (18) to the equations describing the dynamics of the micromechanical structure, we will validate our approach by comparing its results with those of a finite difference code.

3 Validation of the proposed reduced-order model

In order to validate (18-21), we have built a finite-difference model of (2), based on a backward-Euler approximation. We also use this approximation scheme for (18). Since $\mathbf{A}$, $\mathbf{H}$ and $\mathbf{f}$ do not depend on the squeeze coordinates, the backward-Euler approximation yields the following recurrence equation:

$$\mathbf{s}^{n+1} = \left(\mathbf{A}^{n+1} - \Delta t \mathbf{H}^{n+1}\right)^{-1}\left(\mathbf{A}^n \mathbf{s}^n + \mathbf{f}^{n+1} - \mathbf{f}^n\right), \qquad (22)$$

where Δt is the chosen time-step and the notation $\mathbf{X}^n$ stands for $\mathbf{X}(n\Delta t)$. In Fig. 1, we show a comparison of the results obtained with the two models for different values of the squeeze-number. We choose the following numerical values: $L=310\times10^{-6}$ m, $W=40\times10^{-6}$ m, $G_0=2.3\times10^{-6}$ m, $\mu=1.82\times10^{-5}$ Pa.s, $P_0=10^5$ Pa. The excitation is of the form:

$$G_\alpha(x,t) = G_0\left(1 - \alpha W(x)\cos(\omega t)\right), \quad (23)$$

with $\omega=3\times10^5$ rad.s^{-1}, and

$$W(x) = 16\left(\frac{x}{L}\right)^2\left(1-\frac{x}{L}\right)^2, \qquad (24)$$

so that $W(L/2)=1$. Coefficient α varies between 0 and 1. The boundary conditions are chosen as open on all sides ($p=0$). A 50×40 mesh is used for the finite difference scheme, whereas 6 modes are used for the reduced-order model. 400 time-steps are used to discretize one period of the excitation. Fig. 1 shows that there is a very good agreement between the two models, even for large values of α. Note that when $\alpha=0.8$, the maximum pressure is about 3×10^4 Pa, which is out of the domain of validity of both models, even though the squeeze number for the chosen parameters is of the order of 10 (and the Reynolds number is of the order of 0.1). This goes to show that the squeeze number is mostly relevant for the study of squeeze film under small uniform displacements: in the case of large, non-uniform displacements, it is much more difficult to define a characteristic length and a characteristic gap. In annex A, a more complete study of the domain of validity of the small pressure approximation is given.

It appears, from simulating the system for different sets of parameters, that the number of modes necessary to capture the behaviour of the squeeze film depends mostly on four factors: the regularity of $W(x)$, the aspect ratio of the micromechanical structure, the squeeze number and the amplitude of the excitation. In the most favourable conditions, 1 or 2 modes are enough. We show in annex B that other choices of basis functions do not lead to such a compact representation of the solution of the original problem.
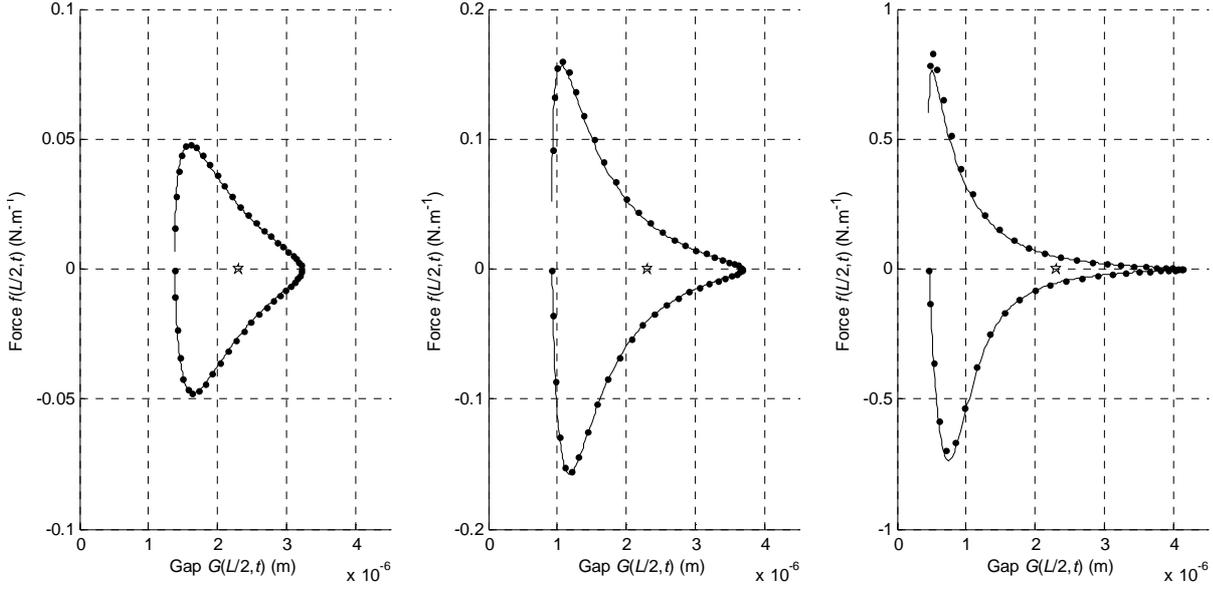
Fig. 1- Comparison of the finite difference model (dots) with the reduced-order model (continuous line). The results correspond, from left to right, to $\alpha = 0.4$, $\alpha = 0.6$ and $\alpha = 0.8$. The curves represent the value of the force per unit length at the middle of the bridge, i.e. $f(L/2,t) = \int_0^W p(L/2, y, t)dy$, versus $G_\alpha(L/2, t)$.

III Coupled simulation of deformable structures

For a structure under electrostatic actuation, one may usually write:

$$\mathbf{K}(\mathbf{x})\mathbf{x} + \mathbf{M}\ddot{\mathbf{x}} = \mathbf{p}^e + \mathbf{p}^{flu}, \quad (25)$$

$\mathbf{x}$ being the mechanical (modal) coordinates, $\mathbf{K}(\mathbf{x})$ the possibly nonlinear stiffness matrix, $\mathbf{M}$ the mass matrix, and $\mathbf{p}^e$ (respectively $\mathbf{p}^{flu}$) the projection of the electrostatic (respectively fluidic) pressure on the mechanical modes. Letting $\xi_l(x,y)$ be the lth mechanical mode, we have:

$$p_l^{flu} = \sum_{k=1}^N \left\langle \varphi_k G^{-3/2} \middle| \xi_l \right\rangle s_k(t) = \sum_{k=1}^N B_{lk} s_k(t) . \qquad (26)$$

Thus, (25) may be rewritten as:

$$\frac{d}{dt}\left(\begin{bmatrix} \mathbf{I} & 0 & 0 \\ 0 & \mathbf{M} & 0 \\ 0 & 0 & \mathbf{A} \end{bmatrix} \begin{bmatrix} \mathbf{x} \\ \dot{\mathbf{x}} \\ \mathbf{s} \end{bmatrix} - \begin{bmatrix} 0 \\ 0 \\ \mathbf{f} \end{bmatrix} \right) = \begin{bmatrix} 0 & \mathbf{I} & 0 \\ -\mathbf{K} & 0 & \mathbf{B} \\ 0 & 0 & \mathbf{H} \end{bmatrix} \begin{bmatrix} \mathbf{x} \\ \dot{\mathbf{x}} \\ \mathbf{s} \end{bmatrix} + \begin{bmatrix} 0 \\ \mathbf{p_e} \\ 0 \end{bmatrix} . \qquad (27)$$

One may introduce some modified squeeze coordinates $\tilde{\mathbf{s}}$ in order to make (27) more tractable:

$$\tilde{\mathbf{s}} = \mathbf{A}\mathbf{s} - \mathbf{f} . \qquad (28)$$

Equation (25) is then equivalent to:

$$\frac{d\mathbf{u}}{dt} = \begin{bmatrix} 0 & \mathbf{I} & 0 \\ -\mathbf{M}^{-1}\mathbf{K} & 0 & \mathbf{M}^{-1}\mathbf{B}\mathbf{A}^{-1} \\ 0 & 0 & \mathbf{H}\mathbf{A}^{-1} \end{bmatrix} \mathbf{u} + \begin{bmatrix} 0 \\ \mathbf{M}^{-1}\mathbf{p_e} + \mathbf{M}^{-1}\mathbf{B}\mathbf{A}^{-1}\mathbf{f} \\ \mathbf{H}\mathbf{A}^{-1}\mathbf{f} \end{bmatrix} = \mathbf{G}(\mathbf{x})\mathbf{u} + \mathbf{g}(\mathbf{x}), \qquad (29)$$

where

$$\mathbf{u} = \begin{bmatrix} \mathbf{x} \\ \dot{\mathbf{x}} \\ \tilde{\mathbf{s}} \end{bmatrix} \qquad (30)$$

is the state of the coupled system. The solution to evolution equation (29) can then be approximated using a numerical technique. We consider in the rest of the paper that the dimension of $\mathbf{u}$ is $2M+N$, where M is the number of mechanical modal coordinates and N is the number of squeeze coordinates.

1 Practical considerations

Before moving to the validation of this reduced-order model, we make a few comments concerning its practical implementation. First of all, notice that the evolution matrix $\mathbf{G}$ does not depend on the complete system state but only on the mechanical modal coordinates, and that the same goes for $\mathbf{g}$. This is as opposed to the reduced-order models based on the nonlinear Reynolds equation, where the evolution matrix depends not only on $\mathbf{x}$ but also on the pressure modal coordinates and, in some cases, on $\dot{\mathbf{x}}$. The practical importance of this remark is clear when one estimates the cost of the numerical integration of (29): at each time-step, the state-dependent coefficients of $\mathbf{G}$ and $\mathbf{g}$ must be evaluated at least once, depending on the complexity of the numerical integration scheme. This means that, at each time-step, all the quantities appearing in (19-21) and (26) must be calculated and the corresponding two-dimensional integrals must also be computed. This issue is addressed in [17-18], where a piecewise-linear approach to the reduced-order modelling of MEMS is proposed. A similar technique may be used in the present case, i.e. instead of solving (29), one can try to find an approximation $\hat{\mathbf{u}}$ of the solution which verifies:

$$\frac{d\hat{\mathbf{u}}}{dt} = \hat{\mathbf{G}}(\mathbf{x})\hat{\mathbf{u}} + \hat{\mathbf{g}}(\mathbf{x}), \qquad (31)$$

where $\hat{\mathbf{G}}$ and $\hat{\mathbf{g}}$ are piecewise-linear approximations of $\mathbf{G}$ and $\mathbf{g}$. One should then evaluate $\mathbf{G}$ and $\mathbf{g}$ for a chosen set of values of $\mathbf{x}$ and find the corresponding piecewise-linear interpolation in the M-dimensional space of mechanical modal coordinates. Now, if $\mathbf{G}$ and $\mathbf{g}$ also depended on $\dot{\mathbf{x}}$ and on the squeeze coordinates, they would exist in a $(2M+N)$-dimensional space and, consequently, their piecewise-linear approximations would be costlier to establish and to store.

Another reason why the structure of the proposed reduced-order model is advantageous becomes apparent when one uses an implicit integration scheme for solving (29) or (31). For example, the backward-Euler method with time-step Δt gives:

$$\mathbf{r}\!\left(\mathbf{u}^{n+1}\right) = \left(\mathbf{I} - \Delta t\mathbf{G}\!\left(\mathbf{x}^{n+1}\right)\right)\mathbf{u}^{n+1} - \Delta t\mathbf{g}\!\left(\mathbf{x}^{n+1}\right) - \mathbf{u}^{n} = \mathbf{0}. \quad (32)$$

Solving (32) for $\mathbf{u}^{n+1}$ calls either for a predictor-corrector method or for some Newton-Raphson iterations. In the latter case, one needs to compute $\mathbf{J}$ the Jacobian of $\mathbf{r}$ at each Newton iteration step. The coefficients of the Jacobian matrix are given by:

$$J_{kl} = \frac{\partial r_k}{\partial u_l}. \qquad (33)$$

The particular structure of the proposed model can then be put to good use, because, $\mathbf{x}$ being constant, $\mathbf{r}$ is linear with respect to $\dot{\mathbf{x}}$ and $\tilde{\mathbf{s}}$. Thus, the part of the Jacobian matrix corresponding to the partial derivatives with respect to $\dot{\mathbf{x}}$ and $\tilde{\mathbf{s}}$ can be expressed very simply as a function of $\mathbf{G}$. The remaining part can be approximated using finite differences in M-dimensions. Moreover, if $\mathbf{G}$ and $\mathbf{g}$ are piecewise-linearly approximated, the partial derivatives of $\hat{\mathbf{G}}$ and $\hat{\mathbf{g}}$ with respect to $\mathbf{x}$ are constant and known on each sub-domain of the M-dimensional space, which makes for an even simpler evaluation of the Jacobian.

2 Validation of the coupled model

We validate our approach with the classical test case described in [14-16], which is also used as a basis for comparison in [17-18]. The characteristics of the micromachined switch are the following: L=610×10^{-6} m, W=40×10^{-6} m, h (thickness) =2.2×10^{-6} m, G_0=2.3×10^{-6} m, μ=1.82×10^{-5} Pa.s, P_0=1.013×10^5 Pa, E (Young's modulus) =149×10^9 Pa, S (residual stress) =-3.7×10^6 Pa, ρ (density) =2330 kg.m^{-3}, ε_0 (permittivity of vacuum)=8.854×10^{-12} F.m^{-1}. For this set of parameters, the assumption that the losses are dominated by squeeze film damping can be made: for example, a simple calculation based on the "dish model" developed in [1] for drag force damping shows that, for the considered structure, the forces due to squeeze film damping are about one thousand times as large as those due to drag force damping, because $h \ll W$. Moreover, one can estimate the quality factor of the first vibration mode of the beam by assuming small displacement amplitudes and neglecting damping phenomena other than squeeze film: this yields a quality factor smaller than unity and shows that squeeze film plays an important role in the transient dynamics of the structure. As a consequence, the microswitch can be described by the following system of equations:

$$\begin{cases} EI\dfrac{\partial^4 G}{\partial x^4} - S\dfrac{\partial^2 G}{\partial x^2} = F_{elec} + F_{air} \\ \nabla\left((1+6K)\dfrac{G^3}{12\mu}\nabla p\right) = \dfrac{\partial}{\partial t}\left(G\left(1+\dfrac{p}{P_0}\right)\right) \end{cases}, (34)$$

where $F_{elec} = -\varepsilon_0 W V^2 / 2G^2$ is the electrostatic force and $F_{air} = \int_0^W p\,dy$ is the fluidic force. Note that the Reynolds equation has been linearized with respect to pressure. Moreover, the spatial variations of the Knudsen number $K = \lambda/G$, where λ=0.064×10^{-6} m is the mean-free path of air at ambient pressure, are taken into account.

The first equation of (34) is reduced with a Galerkin projection on the first M eigenmodes of the linear spatial differential operator. The second equation is first transformed into a more amenable form, as in section II, by defining an "effective squeeze function" φ as:

$$\begin{cases} \varphi = p\psi(G), \\ \psi(G) = (1+6K)^{1/2}G^{3/2} \end{cases}. \qquad (35)$$

Provided the "small pressure" hypothesis holds, this change of variables yields the following equation:

$$\Delta\varphi - \dfrac{\Delta\psi}{\psi}\varphi = 12\mu\dfrac{\partial}{\partial t}\left(I_\psi + \dfrac{G\psi^{-2}}{P_0}\varphi\right), (36)$$

where I_ψ is the primitive of the inverse of $\psi(G)$, i.e. $I_\psi = \int \psi^{-1}dG$. When $\psi(G)$ is given by (35), we have:

$$I_\psi = \sqrt{\dfrac{2}{3\lambda}}\tanh^{-1}\left(\sqrt{1+\dfrac{1}{6K}}\right). \qquad (37)$$

Note that when another expression is used for the effective viscosity (see, for example, [5]), it is still possible to find a change of variables that transforms the Reynolds equation into (36), as well as an analytical expression for I_ψ.

Now equation (36) can be reduced with a Galerkin projection on N eigenmodes of the Laplacian operator. In the case of a rectangular switch with fixed ends, these squeeze modes are given by:

$$\begin{cases} \varphi_k(x,y) = \phi_{k_1,k_2}(x,y) = \dfrac{C_{k_1}}{\sqrt{LW}} \cos\left(k_1 \dfrac{\pi}{L} x\right) \sin\left(k_2 \dfrac{\pi}{W} y\right) \\ C_{k_1} = \begin{matrix} 2 \text{ if } k_1 \neq 0 \\ \sqrt{2} \text{ otherwise} \end{matrix} \end{cases}, \quad k_1 \geq 0, k_2 \geq 1. \qquad (38)$$

The resulting nonlinear system of ODEs can then be recast in the same form as (29) and solved with a simulation tool.

We show in Fig. 2 the pull-in time t_{pi} of the device versus the applied voltage. These results, obtained with 2 mechanical modes and 3 squeeze modes, fit almost perfectly those of [16]. In [16], it is shown that a similar degree of accuracy can be obtained by using the same number of POD modes (2 mechanical and 3 pressure POD modes): however, these are obtained at a greater cost (simulation time, data storage). Our results also tend to be closer to the experimental data for small values of the actuation voltage: this might be due to the fact that the POD modes in [16] were generated using simulations with voltages no lower than 9 V, although one can assume the shapes of the POD modes change a lot in the critical region close to the pull-in voltage (V_{pi}=8.7 V). Since our model and the one in [16] do not take beam-lengthening into account, the experimental pull-in time is underestimated.

We show in Fig. 3 the maximal pressure variation recorded in these simulations for $t \in \left[0, 0.9 \times t_{pi}\right]^2$: this maximum is always obtained for $t = 0.9 \times t_{pi}$. This quantity increases with the applied voltage and it is usually small compared to the ambient pressure, thereby validating our "small pressure variations" hypothesis. This hypothesis also holds for smaller values of P_0, because the amplitude of the pressure variation is directly linked to the value of the effective viscosity, which decreases with P_0: for example, when P_0 is set to 10^3 Pa and the actuation voltage spans the same range as in Fig. 2, the maximum pressure variation is comprised between 150 Pa and 250 Pa. There is a qualitative difference between the curve corresponding to $P_0 = 10^3$ Pa and the other two, which probably stems from the fact that, at low ambient pressure, the flow is compressible regardless of the voltage.

For lower values of P_0, the small pressure hypothesis no longer holds but the reduced-order model still manages to give accurate pull-in times: this is simply due to the fact that, for very low values of P_0, squeeze-film damping no longer plays a major role in the transient dynamics of the microswitch. Thus, at extremely low ambient pressures, the switching time is correctly predicted, no matter how inaccurate the model may be. This is illustrated in Fig. 4, where the pull-in times obtained for P_0=6×10^{-1} Pa are compared to the experimental and simulated results in [14], and to the switching times obtained when assuming F_{air} =0 in (34).

The relative importance of fluid forces and electrostatic forces at different values of the ambient pressure is also illustrated in Fig. 5: at P_0=1.013×10^5 Pa, the flow is completely incompressible and the electrostatic and the fluidic pressures are comparable. As the ambient pressure diminishes, the flow becomes compressible and the electrostatic pressure becomes larger than the fluidic pressure. These results are qualitatively comparable to those presented, for example, in [21-22] for a nonuniform cantilever microswitch (although, in these references, the small pressure hypothesis does not hold). Note that the threshold pressure for which the flow becomes compressible is highly dependent on the geometry of the structure. In the present case, neglecting compressibility typically leads to relative errors of the order of 20% on the calculated pull-in times (Fig. 6).

---

[2] The reason why the interval chosen for recording the maximum pressure variation is limited to $t \in \left[0, 0.9 \times t_{pi}\right]$ is that, when the gap goes to zero, the pressure variation calculated by our model goes to infinity. For very small gaps, the electrostatic pressure also goes to infinity and keeps the switch in motion.

Finally, the influence of slip-flow effects is illustrated in Fig. 7. These results (obtained with three squeeze modes and two mechanical modes) clearly show the importance of accounting for slip-flow in the study of pull-in dynamics, as pointed out in [23-24]. More illustrations of the role played by rarefaction effects can be found in annex A.
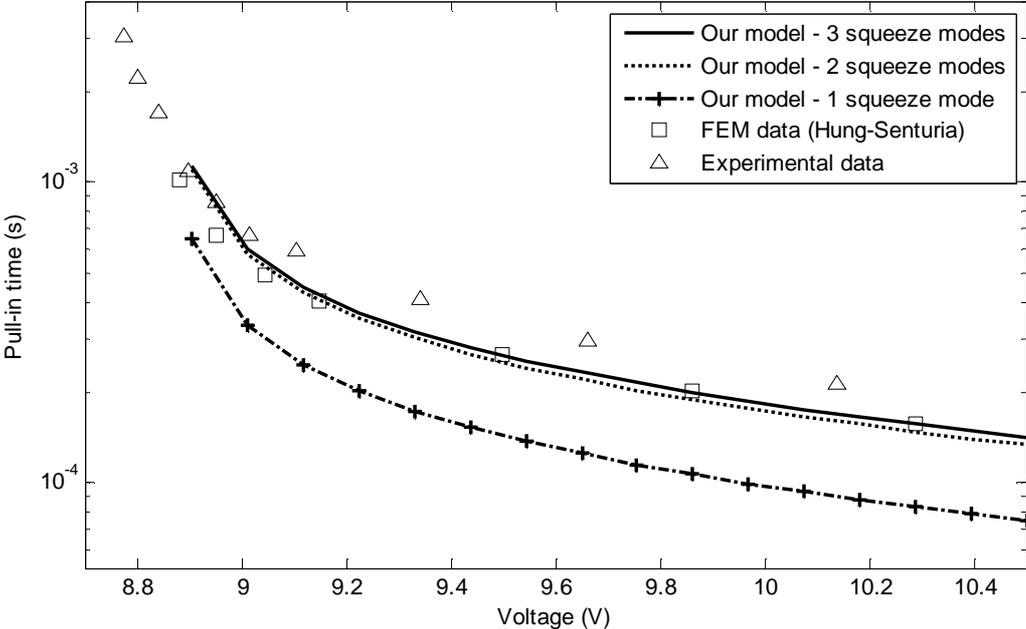

Fig. 2 - Pull-in time (s) versus applied voltage (V) for $P_0 = 1.013 \times 10^5$ Pa. Comparison of the experimental and simulated results presented in [16] to the simulated results obtained with our reduced -order model. The chosen squeeze modes correspond to $k_1 = 0, 1, 2$ and $k_2 = 1$ in (38). For the mechanical part, the first two eigenmodes are used.
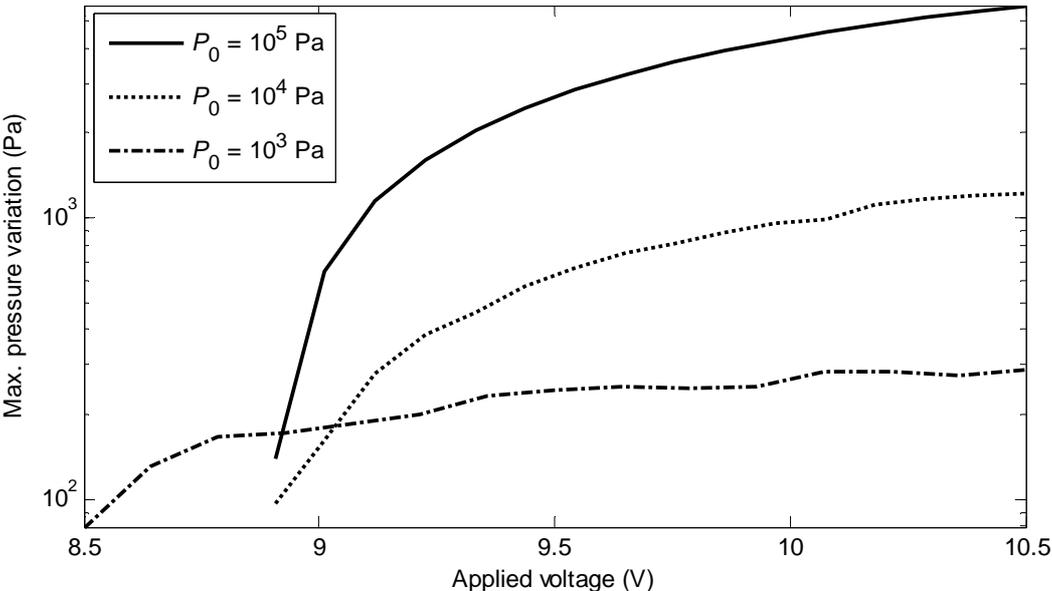

Fig. 3 - Maximal pressure variation (Pa) versus applied voltage (V) for three different values of the ambient pressure.
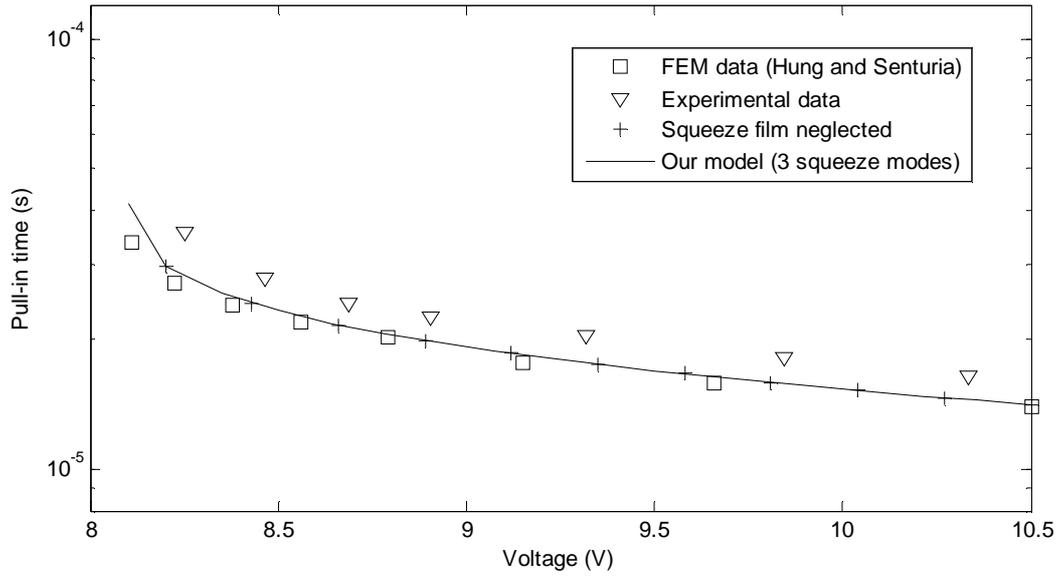
Fig. 4 - Pull-in time (s) versus applied voltage (V) for very low ambient pressure. Comparison of the experimental and simulated results presented in [16] to the simulated results obtained with our reduced -order model, for P_0 =6×10^{-1} Pa. The chosen squeeze modes correspond to k_1 =0, 1, 2 and k_2 =1 in (38). For the mechanical part, the first two eigenmodes are used. The predicted switching times cannot be distinguished from those obtained when completely neglecting damping in (34), i.e. supposing $F_{air} = 0$.
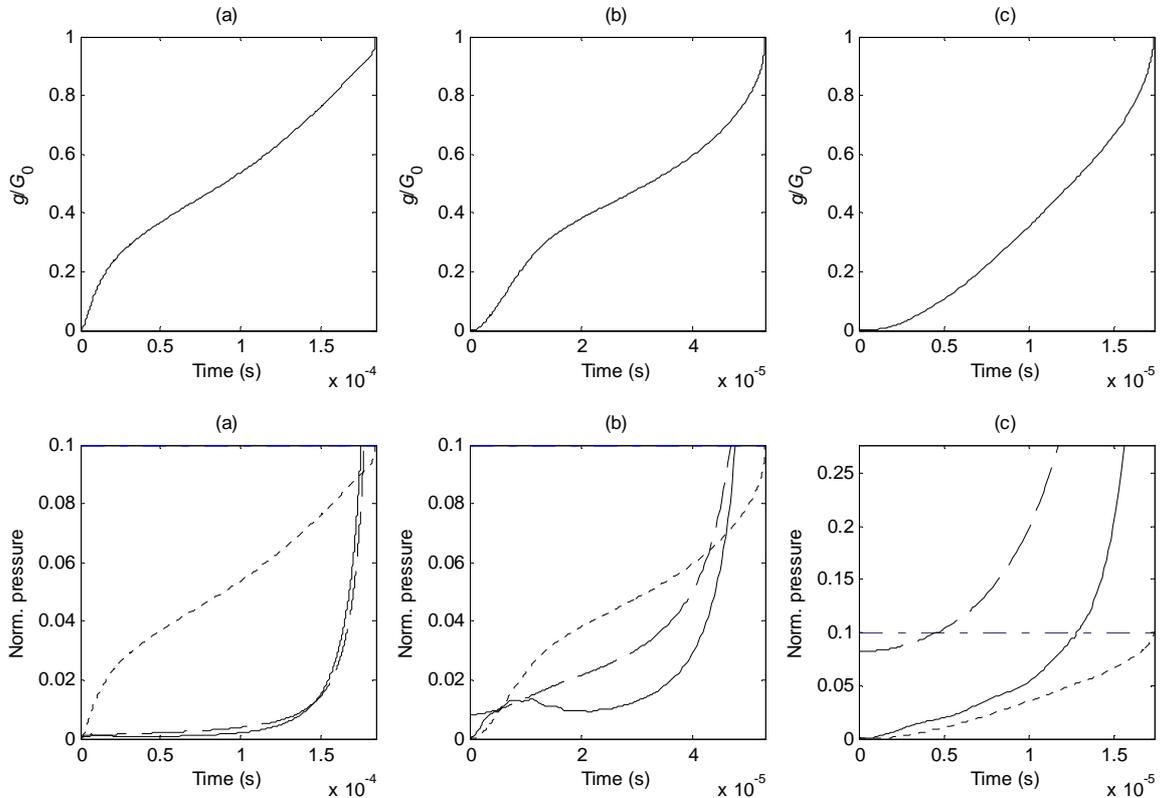

Fig. 5 – displacement of the midpoint of the switch vs. time (s), for P_0 =1.013×10^5 Pa (a), P_0 =1.013×10^4 Pa (b) and P_0 =1.013×10^3 Pa (c) and V =10 V. The displacement is normalized with respect to the gap. In the lower boxes, the corresponding fluidic pressure (continuous line) and electrostatic pressure (dashed line), normalized with respect to the ambient pressure,

are plotted vs. time. The compressibility limit, corresponding to one tenth of the normalized displacements, is also plotted (dotted line), as well as the validity limit of our model (dash-dotted line).
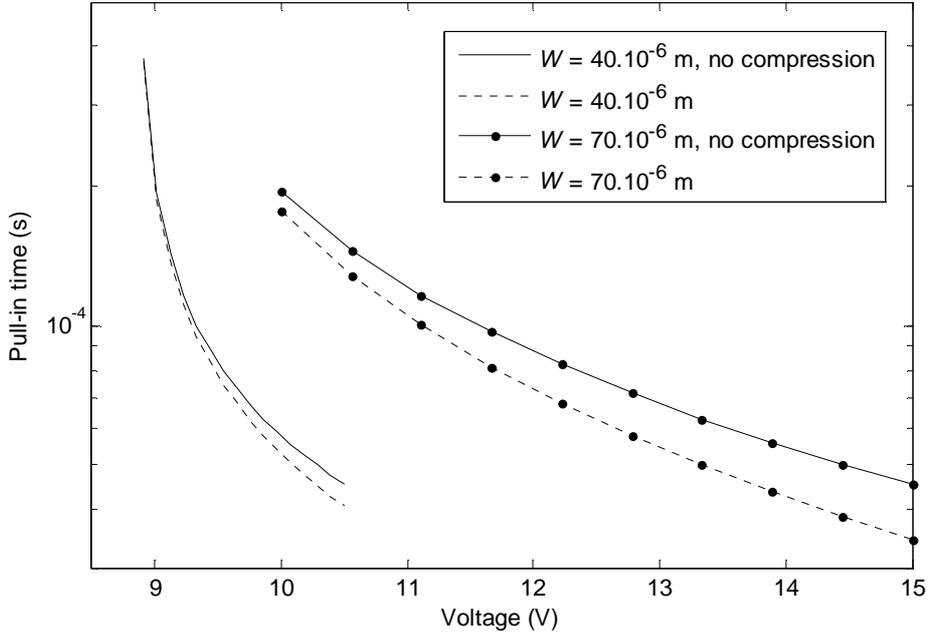

Fig. 6 – influence of compressibility on switching times, for $P_0 = 1.013 \times 10^4$ Pa. The pull-in times calculated with our reduced-order model are represented for two different values of the width of the switch and compared to those obtained when neglecting compressibility.
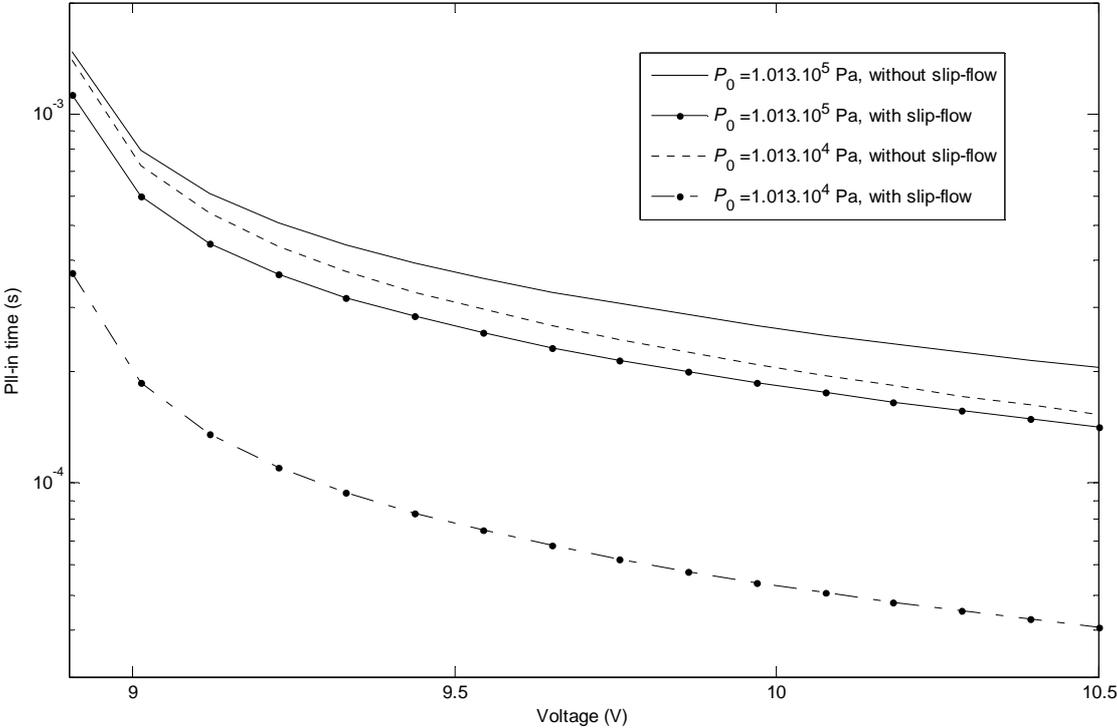

Fig. 7 – pull-in time vs. voltage for different values of the ambient pressure, with and without slip-flow.

IV Conclusion

In the present paper, we have presented a reduced-order model of the squeezed-film damping phenomenon which is valid for:

- flexible structures,
- large displacements (with respect to the gap),
- small pressure variations (with respect to the ambient pressure).

This reduced-order model was validated by comparison to simulated and experimental data taken from [16]. Moreover, we have shown that in several practical cases the "small pressure" hypothesis is not limitative, even when the gap becomes very small.

In order to construct the reduced-order model, we have proposed a change of variables which transforms the Reynolds equation into a more tractable form. This allows us to compute so-called "squeeze modes", for which analytical expressions can be found in simple geometries. In more complex cases (such as plates with holes, for example), the squeeze modes can be found by numerically solving a linear eigenvalue problem. The specificity of this approach, as opposed to those presented in [14-18], is that it does *not* rely on burdensome dynamical simulations of the complete system, nor does it require choosing a training trajectory. Moreover, the linear eigenvalue problem must be solved only once and the resulting squeeze modes are valid regardless of the amplitude of the displacements. Furthermore, we have shown that choosing other projection bases may lead to incomplete representations of the solution of the Reynolds equation.

The main advantage of our reduced-order model is the economy with which it can be established. It is also quite simple to include the effect of a varying effective viscosity coefficient. The practical implementation of our approach is also fairly straightforward and economical, as was shown in section III-1. The main drawback of the proposed approach is that the squeeze modes lack physical significance, making them more difficult to interpret than pressure modes. Another issue lies in the treatment of mixed boundary conditions [3]: this sort of boundary condition does not translate well in terms of squeeze functions. This problem is the subject of ongoing work.

References

[1] M.H. Bao, "Micro mechanical transducers: pressure sensors, accelerometers and gyroscopes", Handbook of Sensors and Actuators, vol. 8, Elsevier, Amsterdam, 2000

[2] T. Veijola et al., "Extending the validity of squeezed-film damper models with elongations of surface dimensions", Journal of Micromechanics and Microengineering, vol. 15, pp. 1624-1636, 2005

[3] A. K. Pandey et al., "Influence of Boundary Conditions on the Dynamic Characteristics of Squeeze Films in MEMS devices", Journal of Microelectromechanical Systems, vol. 16, pp. 893-903, 2007

[4] M.H. Bao, H. Yang, "Squeeze film air damping in MEMS", Sensors and Actuators A, vol. 136, pp. 3-27, 2007

[5] T. Veijola et al., "Equivalent-circuit model of the squeezed gas film in a silicon accelerometer", Sensors and Actuators A, vol. 48, pp. 239-248, 1998

[6] J. E. Mehner et al., "Reduced-order modeling of fluid-structural interactions in MEMS based on modal projection techniques", 12th International Conference on Solid-State Sensors, Actuators and Microsystems, 2003, vol. 2, pp. 1840-1843

[7] F. Pan et al., "Squeeze film damping effect on the dynamic response of a MEMS torsion mirror", Journal of Micromechanics and Microengineering, vol. 8, pp. 200-208, 1998

[8] Pu Li et al., "A new model for squeeze-film damping of electrically actuated microbeams under the effect of a static deflection", Journal of Micromechanics and Microengineering, vol. 17, pp. 1242-1251, 2007

[9] M. I. Younis, A. H. Nayfeh, "Microplate Modeling under Coupled Structural-Fluidic-Electrostatic Forces", 7th International Conference on Modeling and Simulation of Microsystems, 2004, pp. 251-254

[10] M. I. Younis, "Modeling and Simulation of Microelectromechanical Systems in Multi-Physics Fields", Virginia Polytechnic Institute, Ph. D. Thesis, 2004

[11] M. I. Younis, A. H. Nayfeh, "Simulation of squeeze-film damping of microplates actuated by large electrostatic load", Journal of Computational and Nonlinear Dynamics, vol. 2, pp. 232-241, 2007

[12] M. I. Younis, A. H. Nayfeh, "A new approach to the modeling and simulation of flexible microstructures under the effect of squeeze-film damping", Journal of Micromechanics and Microengineering, vol. 14, pp. 170-181, 2004

[13] J. Mehner et al., "Simulation of gas damping in microstructures with nontrivial geometries", 11th Annual International Workshop on Micro Electro Mechanical Systems, 1998, pp. 172–177

[14] Y. J. Yang, "Squeeze-film damping for MEMS structures", Ph. D. Thesis, Massachusetts Institute of Technology, 1998

[15] Y. J. Yang et al., "Macromodeling of coupled-domain MEMS devices with electrostatic and electrothermal effects", Journal of Micromechanics and Microengineering, vol. 14, pp. 1190-1196, 2004

[16] E. S. Hung, S. D. Senturia, "Generating efficient dynamical models for microelectromechanical systems from a few finite-element simulation runs", Journal of Microelectromechanical Systems, vol. 8, pp. 280-289, 1999

[17] M. Rewienski, "A Trajectory Piecewise-Linear Approach to Model Order Reduction of Nonlinear Dynamical Systems", Massachusetts Institute of Technology, 1998

[18] M. Rewienski, J. White, "A trajectory piecewise-linear approach to model order reduction and fast simulation of nonlinear circuits and micromachined devices", IEEE Transactions on Computer-Aided Design of Integrated Circuits and Systems, vol. 22, pp. 155-170, 2003

[19] S. L. Sobolev, "Partial Differential Equations of Mathematical Physics", Dover, 1989

[20] C.M. Harris, A.G. Piersol, "Harris' shock and vibration handbook", McGraw-Hill, Inc., New York, NY, 2002

[21] Z. J. Guo et al., "Modeling, simulation and measurement of the dynamic performance of an ohmic contact, electrostatically actuated RF MEMS switch", Journal of Micromechanics and Microengineering, vol. 17, pp. 1899-1909, 2007

[22] B. McCarthy et al. "A dynamic model, including contact bounce, of an electrostatically actuated microswitch", Journal of Microelectromechanical Systems, vol. 11, pp. 276-283, 2002

[23] Z. J. Guo et al., "Modeling and measurement of the dynamic performance of an ohmic contact-type RF MEMS switch", 14th International Conference on Solid-State Sensors, Actuators and Microsystems, 2007, pp. 651-654

[24] A. K. Pandey, R. Pratap, "Coupled nonlinear effects of surface roughness and rarefaction on squeeze film damping in MEMS structures", Journal of Micromechanics and Microengineering, vol. 14 , pp. 1430-1437, 2004

Annex A - Concerning the small pressure hypothesis

There exists no simple way to express the domain of validity of the small pressure hypothesis in the case of large non-uniform displacements of the micromechanical structure. This is made clear in Fig. A-1 where the maximum pressure recorded[3] for a sinusoidal excitation of the mechanical structure (as in section II-3) is plotted versus the squeeze number of the flow, with α varying between 0.3 and 0.4. The geometry of the structure is that of section III-2, i.e. $L = 610 \times 10^{-6}$ m, $W = 40 \times 10^{-6}$ m, $G_0 = 2.3 \times 10^{-6}$ m. For these parameters, the squeeze number at $P_0 = 1.013 \times 10^5$ Pa is given by:

$$\sigma = \frac{12\mu\omega}{P_0}\frac{L^2}{G_0{}^2} \approx 1.5 \times 10^{-4}\,\omega. \qquad \text{(A-1)}$$

Fig. A-1 shows that, as expected, the maximum relative pressure increases with α. It also shows that the small pressure hypothesis remains valid for squeeze numbers of the order of several hundreds (for example, $\sigma \leq 600$ for $\alpha = 0.3$), whereas the incompressibility hypothesis $p << \alpha P_0$ holds in a more restricted domain ($\sigma \leq 150$ for $\alpha = 0.3$). One can also see that, as α increases, the domain of validity of the small pressure hypothesis and that of the incompressibility hypothesis tend to merge.

Another interesting remark is that the domain of validity (of both hypotheses) increases when the ambient pressure decreases (Fig. A-2), as predicted in [24]: this is the direct consequence of rarefaction effects on squeeze-film damping. One can also notice that the cutoff frequency increases with the Knudsen number, whereas it decreases with the oscillation amplitude.
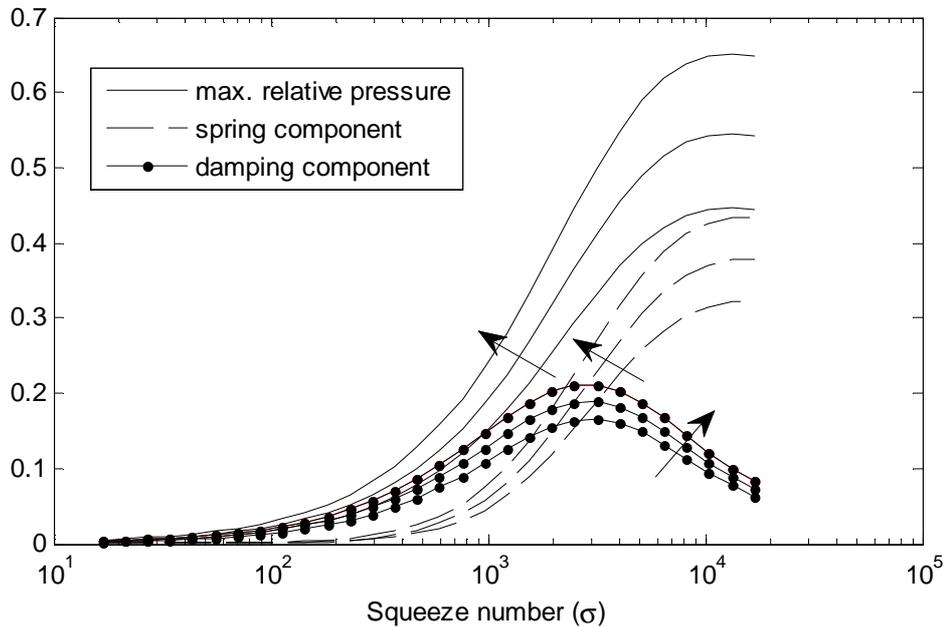

Fig. A-1 - influence of oscillation amplitude on small pressure hypothesis. As α increases from 0.3 to 0.4, the different curves move in the direction of the arrows. The cutoff frequency and the domain of validity decrease with increasing α.

---

[3] These results have been obtained with a finite difference model of the Reynolds equation accounting for rarefaction effects, as in (34).
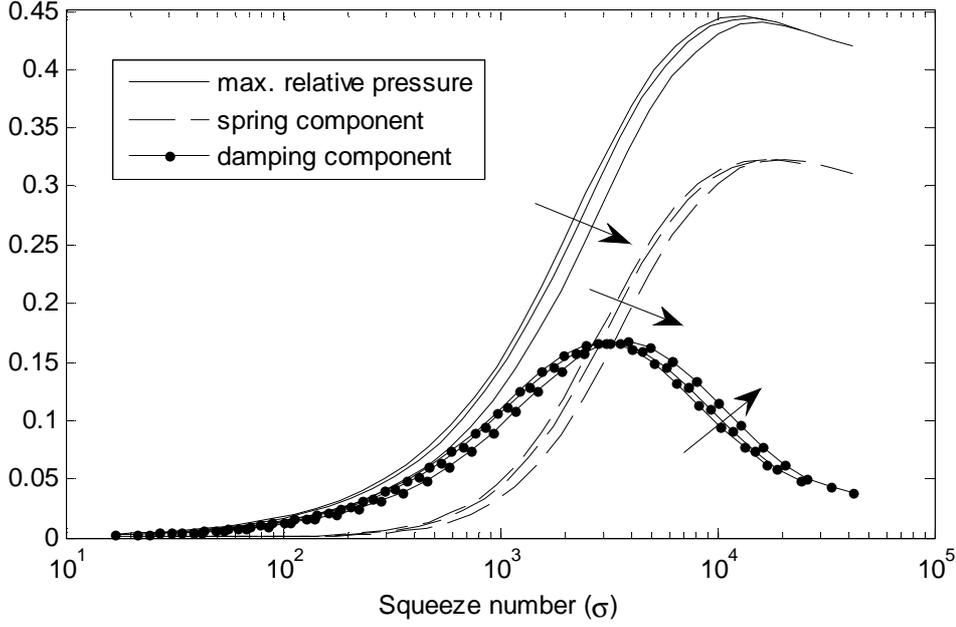
Fig. A-2 - influence of ambient pressure on small pressure hypothesis. As P_0 decreases from 10^5 Pa to $4{\times}10^4$ Pa, the different curves move in the direction of the arrows. The cutoff frequency and the domain of validity decrease with increasing P_0.

Annex B - Concerning the choice of the basis functions

In Fig. B-1, the results obtained with two other reduced-order models are shown, for the same testing conditions as in section II-3. Both reduced-order models are based on Galerkin projections of (2) on the eigenmodes of the Laplacian, i.e. we suppose the solution of (2) can be approximated by:

$$p^{(N)} = \sum_{k=1}^{N} m_k(t) p_k(x, y), \text{(B-1)}$$

with

$$\Delta p_k = -\lambda_k^2 p_k, \text{ (B-2)}$$

and where p_k verifies the boundary conditions. The first model is obtained by projecting (2) on these modes in a very straightforward fashion (as in [16], for example). Since the spatial differential operator in (2) is self-adjoint, we know it should be possible to find a complete basis of modes for this equation if the operator did not depend on time. As it is, there is no way to guarantee that the proposed approximation should converge; in fact, the only way to make sure of convergence is probably to use modes extracted through numerical simulations of (2) for several inputs $G(x, y, t)$, as in [14-18].

In the second model, (2) is "naively" developed into

$$\Delta p + 3(\nabla \log(G)) \nabla p = 12\mu \frac{\partial}{\partial t}\left(G^{-2}\left(-\frac{1}{2} + \frac{p}{P_0}\right)\right), \quad \text{(B-3)}$$

before the projection. The resulting spatial differential operator is not self-adjoint: as a consequence, it is difficult to guarantee that approximations based on the proposed modal decomposition should converge. On the other hand, the second-order derivative of the spatial differential operator no longer depends on time, which might be beneficial.

Both approaches yield reduced-order models structurally similar to (18). The simulations show that, for small variations of G, the two approaches yield good results, although they are

not as accurate as the one proposed in section II. When the variations of G are of the same order as the nominal gap, the accuracy of the two approaches proposed in this annex becomes very poor (Fig. B-1), no matter how many modes are used. On the other hand, the approach based on the transformation to squeeze coordinates remains valid, even for very large deflections (Fig. 1).
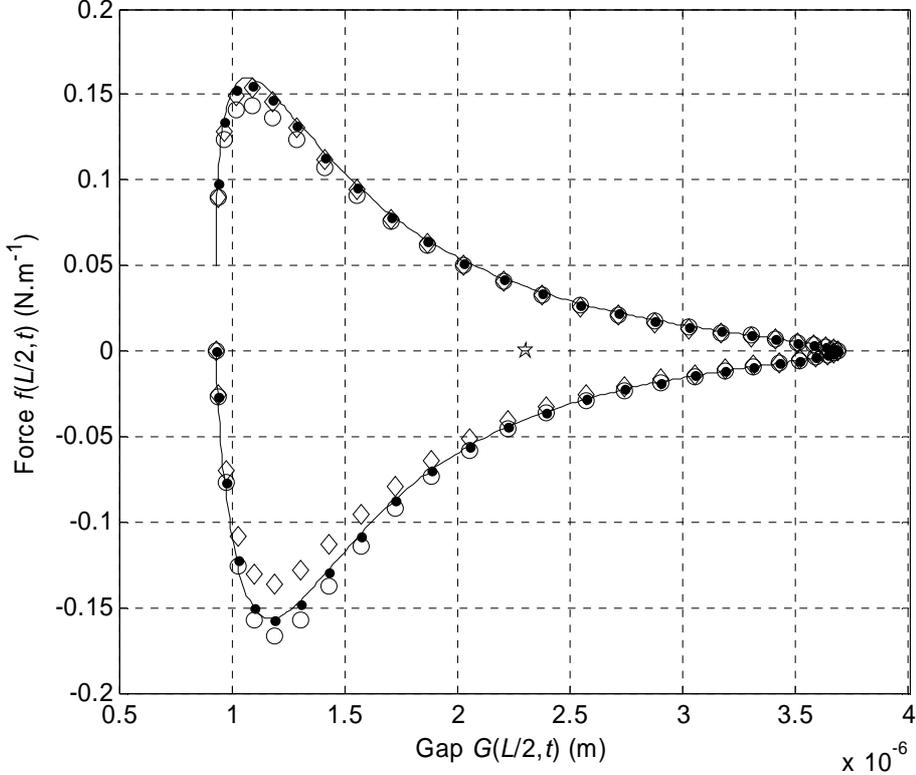

Fig. B-1 - Comparison of the finite difference model (continuous line) with three reduced-order models. The dots correspond to the reduced-order model presented in section II. The circles and the lozenges respectively correspond to the projection of (B-3) and (2) on an orthogonal basis verifying the boundary conditions.